Variable-angle, spectroscopic ellipsometry study based on determining the effect of First Contact Polymer on XeF_2-passivated MgF_2 on Al

Lauren W. Miner[1], Joshua J. Vawdrey[1], Brandon J. Titensor[2], James P. Hamilton[3,4], Richard R. Vanfleet[1], and David D. Allred[1]
[1]Brigham Young University, BYU College of Computational, Mathematical, and Physical Sciences, Department of Physics and Astronomy, N284 ESC, Provo, UT 84602.
[2]Brigham Young University, BYU College of Computational, Mathematical, and Physical Sciences, Department of Statistics, Provo, UT 84602
[3]University of Wisconsin-Platteville, Department of Chemistry, Platteville, WI 53818
[4]Photonic Cleaning Technologies, Platteville, WI 53818

ABSTRACT

Magnesium fluoride on xenon difluoride passivated aluminum (Al+$XeMgF_2$) mirrors have high reflectance encompassing the H Lyman-α at 121.6 nm. Al+$XeMgF_2$ is a key candidate for space telescopes and satellites that demand far-UV (FUV) measurements coupled with high reflectance at longer wavelengths. Contamination can significantly reduce FUV reflectance, so Al+$XeMgF_2$ mirrors must be as clean as possible. Protecting the surfaces while in storage is also desirable. We investigated the suitability of four different formulations of Photonic Cleaning Technologies' First Contact Polymer for cleaning and protecting Al+$XeMgF_2$ coatings by repeatedly cleaning test samples. These were cleaved from a silicon wafer coated with 300 nm of chemical vapor deposited (CVD) silicon nitride (Si_3N_4). All the formulations could clean samples at least once. Using Variable-Angle, Spectroscopic Ellipsometry (VASE), we determined that two (S2 and S3) of the four tested formulations were able to clean and protect the Al+$XeMgF_2$ surfaces multiple times (>20) over 5 months without detectable alumina growth on the Al in a low humidity environment. There were also no changes to the thickness of 'apparent' MgF_2. Apparent MgF_2 includes the deposited MgF_2, the 2–3 nm AlF_3 layer produced by the XeF_2 passivation step, and contributions from surface roughening. There was also no detectable alumina growth for the controls. The fact that the samples were stored between tests in a desiccator with their First Contact overcoat provides evidence that Al+$XeMgF_2$ samples can successfully be protected and stored under some First Contact formulations for at least five months in a dry environment. Far-ultraviolet reflectance is not reported here.

Keywords: First Contact polymer, aluminum, magnesium fluoride coating, Lyman-α, space telescope mirror, ellipsometry, long-term testing

1. INTRODUCTION

The Lyman limit (91.2 nm) to the H Lyman-α (121.6 nm) is crucial to far-ultraviolet (FUV) astrophysical research, opening research avenues in exoplanet atmospheric spectroscopy [1]. Particulate contamination can lead to scattering and molecular hydrocarbon contaminants can significantly decrease mirror reflectivity in the FUV. For example, the Hubble Space Telescope (HST) was predicted to have less than 10% loss of reflectance at H Lyman-α due to contamination throughout ground-based operations [2]. To mitigate reflectance losses from contaminants for space missions, contamination budgets are often established based on specific objectives [3]. Both particulate contaminants (i.e., clothing fibers, dust fragments, etc.) and molecular residues (e.g., organic films from outgassing) are carefully cleaned from mirror surfaces used for space telescope use. Typically, space telescope components are manufactured, assembled, and tested in a cleanroom environment compatible with the cleanliness standard set for the optical system as agreed upon by the project leadership, scientists, and engineers.

To capture light between the Lyman limit and H Lyman-α, the state-of-the-art mirror coating options rely on the high FUV reflectance of aluminum (Al) [4]. Al oxidation after coating is nearly instantaneous upon exposure to air and

UV/Optical/IR Space Telescopes and Instruments: Innovative Technologies and Concepts XII, edited by Jonathan W. Arenberg, H. Philip Stahl, Proc. of SPIE Vol. 13623, 1362308
2025 Published by SPIE · 0277-786X · doi: 10.1117/12.3065884

significantly hampers FUV reflectivity. To mitigate oxidation of the aluminum, a metal fluoride, capping thin-film layer with a high bandgap is deposited on top of the aluminum layer which is transparent in the FUV. The low wavelength cut-off is 115 nm for MgF_2 and 100 nm for LiF [5,6]. The HST used MgF_2 on Al (Al+MgF_2), but a proposed improvement would be utilizing a xenon difluoride (XeF_2) passivation process on the Al in a similar way as used on Al+XeLiF, creating a 2.5 nm protective layer of aluminum fluoride (AlF_3) at the interface of the Al and the deposited fluoride. This XeF_2-passivated MgF_2 on evaporated Al coating is termed Al+$XeMgF_2$ [4]. Al+$XeMgF_2$ has been proven to have higher reflectance than Al+MgF_2, with a lower aging rate and higher chemical stability [4]. However, contamination is a threat to the FUV reflectance on these mirrors. For example, 1 nm of hydrocarbon contamination can absorb 6% to 7% of light at H Lyman-α [6]. Moreover, particulate contamination, even for mirrors stored in cleanrooms, remains a consideration. For a surface cleaned to a particle cleanliness level of 300, particulate contamination can lead to a surface obscuration fraction up to 10^{-4} (e.g., see IEST-STD-1246 [6]). While this fraction is small, it could limit the system performance of high contrast coronagraphy due to light scattering [7].

The ability to clean mirrors reliably to the atomic level is essential. Photonic Cleaning Technologies' Family of Apply-Dry-Peel First Contact™ Polymers (FCP) can clean conventional mirrors of particles and molecular contaminants down to the angstrom level. FCP has been used to clean and also to provide a protective polymer film suitable for storing optical components in a variety of large-scale optical projects, such as those on LIGO [8]. It was also tested on oxide-based coatings [9] and has recently been tested on thin Al+XeLiF [10]. Some FCP formulations are acceptable for cleaning LiF, but none have yet been shown to be suitable for protecting LiF surfaces in long-term storage, though studies are ongoing [10,11].

Here we report on our study of the cleaning and storage of Al+$XeMgF_2$ test samples using the same four formulations explored in the previous Al+XeLiF study [11]. We examined the use of the formulations for both single and repeated cleanings, as well as for long-term storage. Our work was guided by experience with Al+XeLiF. Unlike LiF, MgF_2 is not hygroscopic. However, it is very slightly soluble in water [12]. Our concern is that any polymeric film or coating that uses water – such as the trace amounts of water in FCP - may create thin spots (pores) in the MgF_2 layer through a process termed Ostwald ripening like what has been noted with LiF films [13]. These pores could leave the aluminum in the Al+$XeMgF_2$ layer susceptible to oxidation. Such changes may also cause surface roughening over time, which is detrimental for coronagraphy [7].

We were also concerned about layer blistering and delamination that could be caused by poor film substrate bonding and/or excessive polymer-to-surface adhesion [11]. However, custom tailor-made FCP formulations have previously been produced for materials that cannot be cleaned by the standard formulation. We anticipated that at least one of these custom FCP formulations would not cause substantial changes, possibly due to differences in polymer-to-surface adhesion. This report focuses on the use of ellipsometry and, to a lesser extent, atomic force microscopy (AFM) as characterization tools. Two of the formulations passed the multiple cleaning and five-month storage tests. To what extent FUV reflectance is preserved is the subject of a future report.

2. METHODS

2.1 Sample preparation and constituents

A 200 mm diameter Si wafer (100 orientation) was cleaved at BYU to produce a roughly square piece approximately 150-mm x 150-mm. Because 200 mm times √½ is slightly less than 150 mm, the corners of the square were somewhat rounded. This size was approximately the maximum which could fit in the GSFC chamber. This silicon wafer piece had a coating of ~300 nm of chemically vapor deposited (CVD) Si_3N_4 which aided in ellipsometric characterization as explained below. At NASA-GSFC code 5510, the Al+$XeMgF_2$ layers were deposited, and the wafer piece was returned to BYU. After the coated wafer was received at BYU, test samples (about 1" x 1" samples) were cleaved for the experiments. A schematic cross section of the anticipated films comprising the coating and the substrate is shown in Figure.1. As determined by ellipsometry, the Al was around 25 nm thick, and the actual fluoride thickness (mostly MgF_2) was around 14 nm. The standard thicknesses of layers for space mirrors using MgF_2 on Al are 25 nm and >70 nm, respectively. In addition, the passivation process produces a 2 to 3 nm AlF_3 layer [5]. We used 2.5 nm for the AlF_3 thickness. Due to the larger affinity of F for Al, it is unlikely that any oxide formed on the Al [4,5]. Therefore, the aluminum oxide layer thickness was assumed to be roughly zero upon fabrication and upon our receiving the sample. Note that by design the Al was deliberately made about 70% thinner than that used in actual 'flight' mirrors. When the

Al is thin, the ellipsometer's light can penetrate the film and reflect off the entirety of the optical stack. This is particularly true in the UV.
Depositing the Al+$XeMgF_2$ on a Si_3N_4 layer rather than a 'bare' silicon wafer may seem like an extra complication. The 300 nm of silicon nitride is chosen to produce interference fringes in the Ψ and Δ spectra, allowing convenience for fitting film thicknesses for layers above it with high precision, particularly for partially absorbing films such as the Al film. The technique is known as interference enhancement [14]. There is no reason to expect that having somewhat thinner coatings will significantly affect the validity of these "cleaning" studies for Al+$XeMgF_2$ mirrors, although this should be verified.

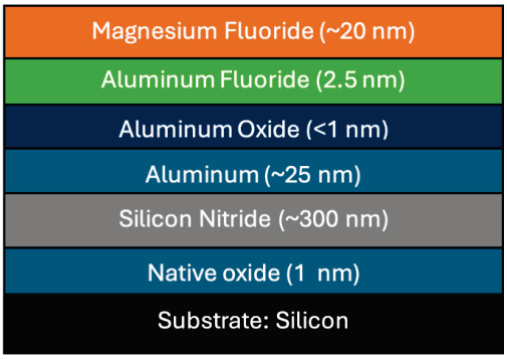


Figure 1. Model of the thin-film stack of the thin Al+$XeMgF_2$ used in this study. Al is deposited by vacuum evaporation, and AlF_3 is formed from a XeF_2-passivation process which immediately follows the Al deposition. Without breaking vacuum, MgF_2 is deposited by evaporation *in situ* as a capping layer [4]. Prior to cycling tests, the aluminum oxide layer is taken to be absent.

2.2 Cleaning and storage studies

In this study, we define a 'peel-off cycle' as a process consisting of the following steps: (1) removing the FCP layer by embedding FC-NET, a chemically inserted mesh, into the polymer layer through a second FCP application, (2) performing three VASE measurements at different locations on the sample, (3) applying a specific FCP formulation on the surface of the Al+$XeMgF_2$ to await further peel-off, and (4) storing the sample in a desiccator maintained at <18% relative humidity (RH) until the designated time for step 1 to be repeated, that is, for the FCP to be removed. Note that the samples are stored with an FCP coating when not being measured. Thus, these studies provide data on the storage of MgF_2 coated Al mirrors with an FCP coating in a dry ambient, though this was not the primary purpose of the study when it began. It should also be noted that we initially took three ellipsometric measurements per sample per cycle, but this was later increased to six measurements.

2.3 Variable-Angle, Spectroscopic Ellipsometry (VASE), modeling and obtaining optical constants

To characterize the changes that Al+$XeMgF_2$ underwent with single and repeated FCP applications, variable-angle spectroscopic ellipsometry (VASE) was employed. A multiparameter model was then used to fit layer thicknesses of the thin-film stack corresponding to the experimental Ψ and Δ values, with CompleteEase's generated mean square error (MSE) indicating the fit quality.

A J.A. Woollam RC-2 variable-angle, spectroscopic ellipsometer was employed in these studies. The beam spot is ~1 mm diameter. At higher incident angles (around 75°), the beam spot would be stretched into an ellipse with a major axis of 6 mm and a minor axis of 1 mm. The sample was measured three times along a line along the center of the sample. In the majority of the measurements, the sample was then rotated 90° and then three additional measurements were performed along a line through the sample, giving six total spectroscopic ellipsometer (SE) measurements for that cycle. Each SE measurement corresponds to multiple wavelength measurements at seven different incident angles. The angles of incidence for evaluation are 50° to 80° in 5° increments with an acquisition time of at least five seconds per angle. Our instrument uses white light (193 to 1000 nm) that is initially linearly polarized. The polarization direction of this linearly polarized light is at 45° from both the s- and p-planes as it strikes the surface. The p-plane contains the surface normal and the direction of ray propagation. The s-plane is perpendicular to the p. As the light reflects, the polarized light amplitudes change according to the formula $\tan\Psi\, e^{i\Delta} = \frac{r_p}{r_s}$, where the ratio of the Fresnel coefficients $\frac{r_p}{r_s}$ in the p and s directions is related to Ψ (amplitude) and the difference in phase between the two amplitudes is Δ [15,16].

After ellipsometric data is collected, the measurements were processed using J.A. Woollam's CompleteEase™ software to obtain the thicknesses and, in some cases, the optical constants of various layers. When fitting SE data from dielectric multilayers containing ultrathin layers with similar indices and dispersion, the computed film thicknesses and roughness are strongly (negatively) correlated. Thus, as much as possible in this study, the values of correlated parameters were constrained by other physical observations and prior knowledge. For example, surface roughness can also be determined via AFM and was used to identify surface features and analyze trends in the root-mean-square (RMS) nano-roughness. Moreover, past experience studying fluoride layers via SE was included in the ellipsometry models [11,17]. MgF_2 is a birefringent crystal. Via SE, we cannot tell if these ultrathin films have random or a preferred orientation. In addition, the AlF_3 layer under a thick fluoride layer could not be definitively detected even in the ellipsometric data from fresh, as-prepared samples. Lastly, since the index of AlF_3 and MgF_2, are similar (for example, 1.398 and 1.386 at 3.3 eV), it was difficult to uniquely determine their individual thickness. Therefore, as explained below, we often lumped the AlF_3 and the Al oxide into the MgF_2 as one MgF_2 layer with an 'apparent' thickness.

In analyzing the ellipsometric data from fresh, as-prepared samples the AlF_3 thickness is assumed to be (about) 2.5 nm based on prior experience with the XeF_2-on-Al process [5]. The initial aluminum oxide thickness is assumed to be zero. This allows the MgF_2 layer thickness to be determined. Given these, the question that needed to be answered was, as the samples were stored and subjected to "cleaning", how did these mirror-like samples change? This was first reduced to this question: how did the thickness of each of these layers and the roughness change? There are constraints. For example, once aluminum oxidizes, the oxide does not disappear only to reappear later. Thus, if the alumina layer's thickness changes, it should increase monotonically and in proportion to the Al that disappears (see below). Similarly, the AlF_3 on the Al is protected by the MgF_2, and its thickness can be left constant unless the MgF_2 ceases to be a barrier. However, if the thickness of all three layers (MgF_2, AlF_3 and alumina) and the roughness were fitted with NO thickness constraints, this is NOT what is observed. The apparent thicknesses for the MgF_2, AlF_3 and alumina layers change erratically from one peel-off cycle to the next or, in the case of the control samples, from measurements made from one day to the next.

The bouncing around of thicknesses is due to high (negative) correlation in our VASE models between the layer thicknesses. The computed thicknesses of films with thicknesses much less than the wavelength of light and similar dispersion curves are highly correlated in optical fitting procedures. Since the MgF_2 layer is the thickest of the three layers above the Al, these dielectric layers were modeled as a single MgF_2 layer. When performing VASE analysis, we started by modeling the MgF_2 thin-film layers above the Al as a single dielectric layer. Therefore, in the first analyses for each sample only three thicknesses were fit: the apparent MgF_2 layer, the Al layer, and the CVD Si_3N_4 layer.

To provide the optical constants of the MgF_2 and Al, we performed a multisample analysis (MSA) on the set of samples received from GSFC and used CompleteEase's gen-osc model to fit the optical constants of each of the two layers independently. The gen-osc model allows the user to input any number of oscillators and distribution functions to calculate the approximate optical constants in multisample analysis [14,18]. VASE data from several samples with films with several different thicknesses and/or postdeposition treatment conditions are all analyzed simultaneously. The optical constants are fitted but are constrained to be the same for all samples. Only the Al, the MgF_2 and the Si_3N_4 film thicknesses are allowed to differ between samples. Multiple samples provide additional spectroscopic optical information while only adding one extra fit parameter per sample (thickness). For the Al layer, we utilized an 8-Gaussian-oscillator, gen-osc model previously used for Al+LiF [11]. In this study, the thickness of the Al varied little, only about 1nm from thinnest to thickest. It is known that the optical constants of Al vary depending on thickness and deposition conditions [17,19]. Thus, we refit the Al oscillator parameters for the Al layer in the Al+$XeMgF_2$, The Al optical constants are shown in Fig. 2. For MgF_2 we used a gen-osc with a Gaussian at 15 eV based on MgF_2 optical constants provided by NASA-GSFC.

To constrain the roughness, we performed AFM to provide an initial roughness survey of the surface topology. We acquired three 5 μm × 5 μm and one 10 μm × 10 μm sample scans from random locations with no features visible from the AFM's optical microscope on the surface. The AFM measurements were analyzed in Gwyddion [20], from which we acquired an associated RMS roughness value (the RMS of surface height variations). Large features, such as blisters or dust, were not included in the RMS roughness. As the roughness used in CompleteEase is a Bruggeman effective medium approximation [21], we converted the average RMS roughness value by approximating the roughness thickness

as a box with area of one and a height of a Gaussian with standard deviation equal to the average RMS roughness. We previously calculated that the RMS roughness needed to be multiplied by a factor of 2.51 in order to match the surface roughness 'thickness' used by CompleteEase.

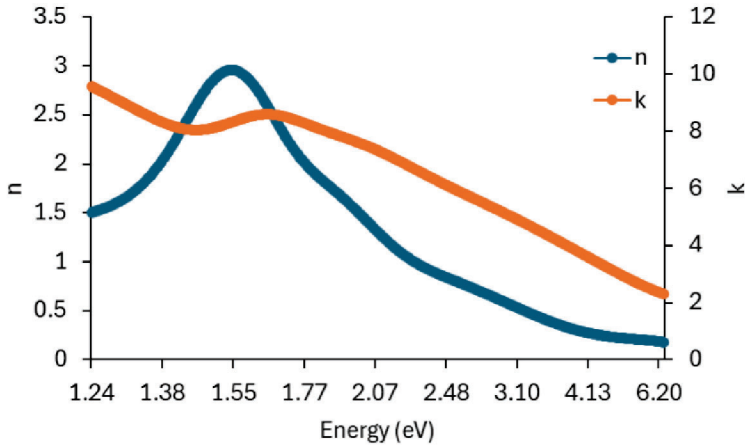


Figure 2. Optical constants used to model the aluminum layer thickness. These were parameterized using an 8-oscillator gen-osc model as described in the text [14].

It was observed that there was a decrease in the Al thickness in some of the Al+XeMgF$_2$ samples as peel-off cycles increased. This decrease can be attributed to oxidation of the Al film producing an aluminum oxide [22]. The value of measuring this decrease for quantifying the growth of the oxide layer cannot be overstated. The question is what are the optical constants and thickness of the layer? The film was too thin to extract optical constants from VASE data in most cases. Therefore, we turn to literature values of alumina or aluminum oxyhydroxide phases. Low-temperature oxidation of aluminum does not produce corundum (sapphire). We hypothesized that the layer resembled alumina deposition at low temperature such as atomic layer deposited (ALD) alumina. Thus, we used the Al_2O_3 optical constants calculated by Shah et al.'s Sellmeier model [23]. As for density we hypothesized that the material would be less dense than sapphire. We used the density of β-Al_2O_3. Using this density and the stoichiometry considerations, we calculated that about 1.54 nm of alumina would form for every 1 nm of Al lost [11].

Our overall objective in these methods was to extract the approximate layer thicknesses of the top-layers of the surface, the MgF_2 layer, as well as that of the alumina layer. By measuring the samples multiple times over extended periods of time, we get a better understanding of how Al+XeMgF$_2$ films fare while being cleaned by, and being stored in, each of the four FCP formulations evaluated.

3. RESULTS AND DISCUSSION INCLUDING STATISTICAL ANALYSIS

We had a limited number of AFM scans to obtain an initial roughness value for each sample and understand morphology after a few applications. Via AFM, the average RMS roughness of all samples at the start of the experiment was 1.17 nm, with a standard deviation of 0.30 nm. After 25 days, the RMS roughness for S1 was 1.26 nm. On day 26, Control 2 had an RMS of 0.96 nm. By day 36, S2 showed an RMS roughness of 1.13 nm. After 46 days, Control 1 and 2 had an RMS roughness of 0.99 and 1.09 nm, respectively. There is insufficient data to calculate any trends for times up to 46 days. It is clear, however, that none of the five RMS values measured at later time differ from the original average by as much as one standard deviation. Four values are smaller, and only one is larger than the initial average. The average of these five measurements is 1.09. Thus, for the first month and a half the roughness does not change for controls and the treated samples as measured by AFM.

The SE model used is that shown in Fig. 1 except the two fluoride layers are combined as one 'apparent MgF_2' layer. To understand our VASE results, we consider the values of three parameters with time – MSE (Fig. 3), MgF_2 thickness (Fig. 5), Al_2O_3 thickness (Fig. 6). We also performed regression analysis to probe the statistical significance of changes that occurred over time. Overall, the FCP application and peel-off proceeded smoothly except for formulation S4. For the first couple of applications, the S4 formulation could be removed easily. However, the time came when a visible portion

of the Al+XeMgF$_2$ layer peeled off with the FCP. This is likely due to excessive polymer-to-layer adhesion or to inadequate cleaning of the substrate prior to Al deposition. Therefore, formulation S4 is not recommended until further studies are completed. However, we found success with two formulations: S2 and S3.

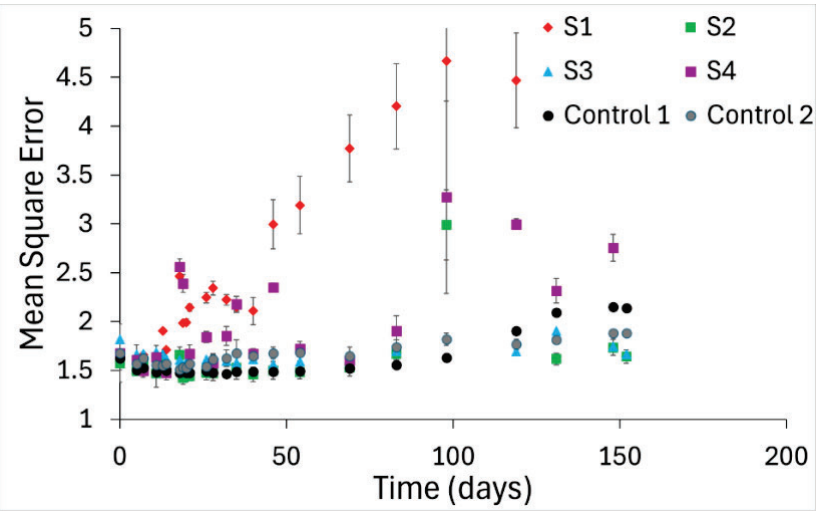


Figure 3. Mean square errors (MSE) from the ellipsometric fit vs. peel-off cycles for six Al+XeMgF$_2$ samples, four different FCP formulations applied and two controls with no FCP applied. The SE model used is shown in Fig. 1. Note that for formulation S1, around 40 days after the initial application the MSE began to increase drastically. Thus, changes to the Al+XeMgF$_2$ sample are so significant that VASE becomes increasingly unsuitable for quantifying change.

Figure 3 shows the MSE for the XeF$_2$-passivated MgF$_2$ on Al (Al+XeMgF$_2$) for the six thin-film stacks as computed via the VASE model. For S1-S4, each data point was taken after the application and removal of one of the four formulations of FCP. The two controls had no FCP applied but were removed from desiccator storage and measured at the same time as the others. Each data point corresponds to the average of three ellipsometric measurements across one of the 1"x1" samples. The uncertainty bars are the standard error of the three measurements. It can be noted in Fig. 3 that the MSE values remain low for all formulations for the first two peel-off cycles. After that MSE for S1 began to increase though the MSE remains below 3 until about day 45. S4 also increased but the rise was not quite so dramatic and the MSE varied from cycle to cycle. The other two samples which are cleaned with an FCP (S2 and S3) remain low, as do the two controls. In fact, by day 150, the MSE of these two cleaned samples is lower than that of the controls. This provides evidence that these two formulations may be compatible with "cleaning the MgF2 surface" many times and that the Al+XeMgF$_2$ sample can be stored in these formulations. However, measurement of FUV reflectance is needed. See discussion of Fig. 4 below.

Figure 4 shows the thicknesses of the 'apparent MgF$_2$ layer' in the XeF$_2$-passivated MgF$_2$ on Al (XeMgF$_2$) for the six thin-film stacks described above as computed via the VASE model. The uncertainty bars are the standard error of the three measurements. Note that the initial values for the thickness are different for each of the six samples. This reflects the fact that they came from different portions of the wafer. The thickness of the layer is highest for portions of the wafer which were closest to the deposition sources. Note that the thicknesses for S2 (squares) and S3 (triangles) and the two controls (filled circles) are relatively constant with time or trend upward only modestly. The increase of apparent fluoride thickness in MgF$_2$ layers with time in air was previously noted by [22] and was attributed to the deposition of adventitious carbon from the air. However, it could also be due to moisture resculpting the surface of the fluoride in the controls. Both processes appear to be blocked in S2. That is, S2 blocks water adsorption on the surface and blocks or removes adventitious carbon. Note further that beyond 40 days the values for samples S1 come from data that is poorly modeled by the CompleteEase model employed, (diamonds in Fig. 3,4, and 6).

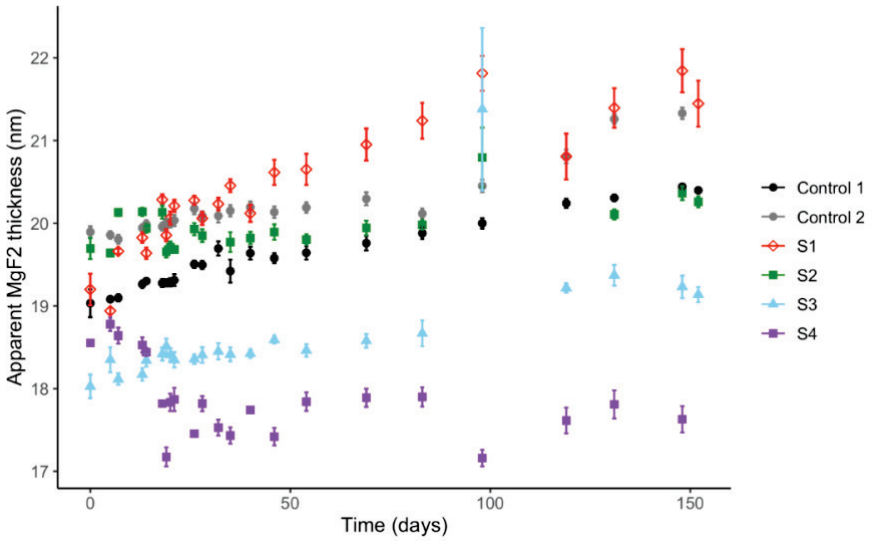


Figure 4. Thicknesses of the 'apparent MgF_2 layer' in the XeF_2-passivated MgF_2 on Al ($XeMgF_2$) for six thin-film stacks as computed via the VASE model. The same symbols are used as in Fig. 3. Each data point was taken after the application and removal of one of the four formulations of FCP for S1-S4. The two controls had no FCP applied but were removed from desiccator storage and measured at the same time as the others. Each data point corresponds to the average of three to six ellipsometry measurements across one of the 1"x1" samples. The uncertainty bars are the standard error of the measurements. Note that the values for S1 come from data that is poorly modeled by the CompleteEase model employed. Measurement angles ranged from 50° to 80° in five-degree increments over the 193-to-1000 nm wavelength range.

The behavior of the MSE for S1 in Fig. 3 at around 40 days after the initial application merits comment. The MSE began to increase drastically. Thus, changes to the Al+$XeMgF_2$ sample were so significant that the model used to interpret the VASE data became increasingly unsuitable for quantifying thickness changes. In Fig. 5A are shown Ψ values (as a function of photon energy) for the S1 Al+$XeMgF_2$ before First Contact applications. B shows Ψ values after approximately 150 days of treatment/multiple First Contact peel offs over the same angles. There are deviations between the model and the data at most energies. The most conspicuous in the increase of Ψ above 5.7 eV seen in 5B. This can be interpreted as the top layer of the stack contains a dispersive material with a transparency edge somewhat beyond 6.5 eV. Replacing the layer with an EMA layer in the model containing MgF_2, voids and water can produce a lower MSE, though not ideal, fit. Water has a slightly lower index (1.344 at 3.3 eV) than the fluorides but possesses a narrower transparency range [24,25]. Its UV absorption is due to the tail of an electronic transition with a maximum at 8.3 eV (149.4 nm) in liquid water This fit is not shown. An MgF_2 surface, is attacked if water is present for several hours.

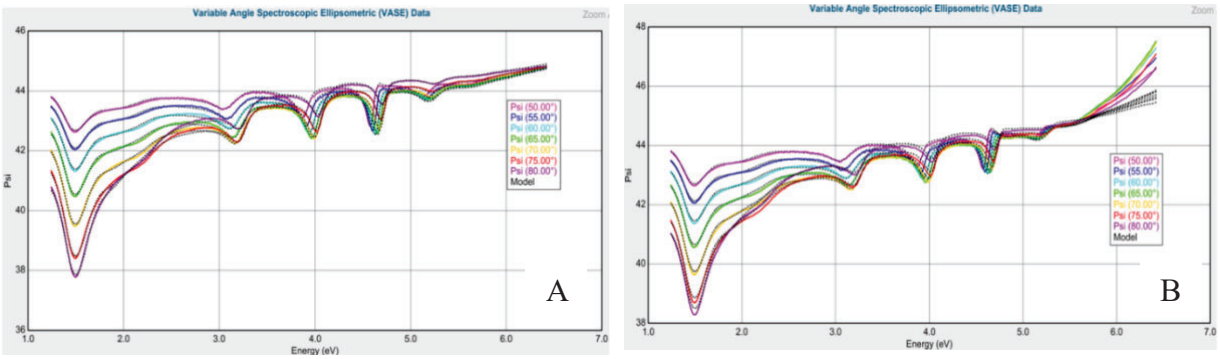


Figure 5. The Ψ (as a function of photon energy) values of the Al+$XeMgF_2$. A shows Ψ before First Contact applications. The seven curves show Ψ for seven angles of incidence from 1.2 to 6.5 eV (193 nm to 1000 nm). Data for 55° is the highest of these curves on the left and for 80° is the lowest. B shows data after approximately 150 days of treatment/multiple First Contact peel offs. The increase of Ψ above 5.7 eV indicates the presence of a dispersive material that may be highly absorbing beyond 6.5 eV as discussed in the text.

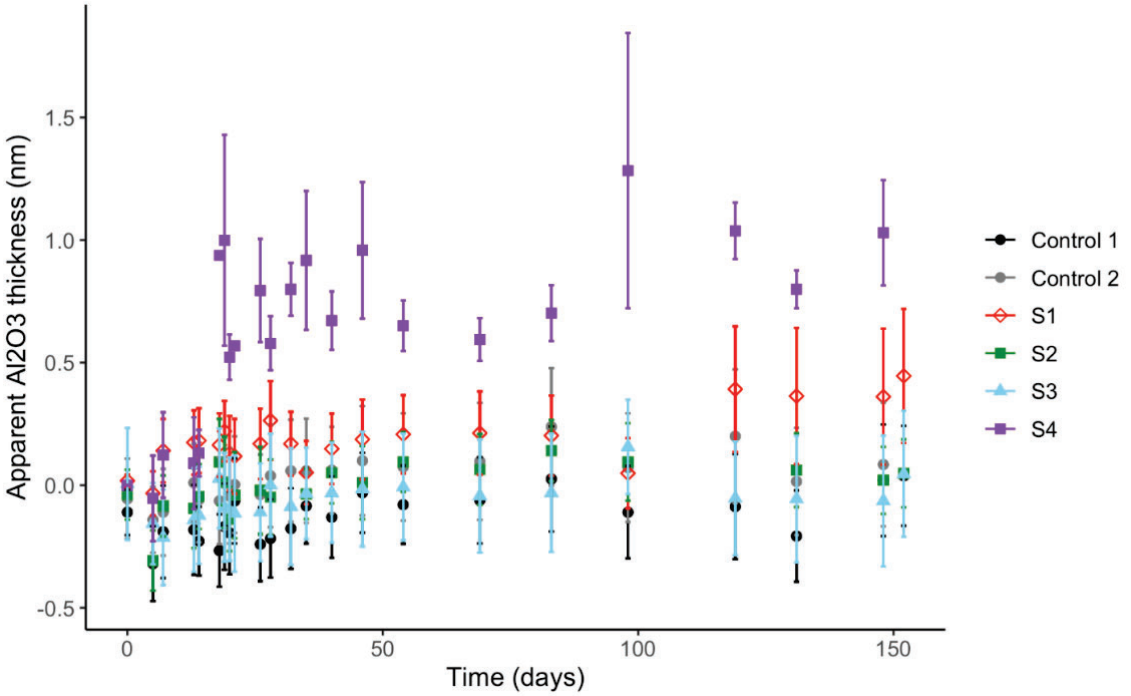


Figure 6. Al_2O_3 thickness of XeF_2-passivated MgF_2 on Al ($XeMgF_2$) as calculated from VASE data using CompleteEase. Each data point was taken after the application of one of four current formulations of FCP. The data measured from a control sample at the same peel-off count as the coated samples is plotted for comparison. Each data point corresponds to three measurements across ~1" x1" samples with measurement angles 50° to 80° in 5-degree increments over the spectral range of 193-to-1000 nm. The "error bars" shown are the standard error of the modeled thickness values from the three measurements.

The growth of alumina as calculated from the disappearance of Al in the VASE model is shown in Fig. 6. Note that no alumina growth over time is seen for S2 (squares), S3 (triangles), or the two controls (filled circles). Also, note that the alumina thickness jumps up after the 6th peel-off for S4. This is the sample which showed some film delamination at the fourth peel off.

4. STATISTICAL ANALYSIS AND DISCUSSION

We performed statistical analysis to investigate trends that may have occurred with the samples. We performed an autocorrelation analysis and a linear regression analysis as a function of (a) peel-off, (b) time in days and (c) logarithmic time.

Autocorrelation allows us to understand if there is dependence on previous measurements in our time series. The Durbin-Watson test showed that there was strong autocorrelation in the MgF_2 layer thicknesses for all samples ($p < 0.001$). A small p provides evidence against the null hypothesis, that is, the observed data is unlikely to have occurred by chance alone. This was found to be most pronounced for formulations S3 (DW stat 0.53) and S4 (DW stat 0.66). As for the alumina layer, S1 and S4 saw significant autocorrelation (S1 $p = 0.002$, S4 $p = 0.047$), but all the others did not. This is consistent with our understanding of the layer thicknesses: As time goes on, the top layer will appear to change since the ellipsometric model lumped several thicknesses into the top layer. These include swelling in the MgF_2 layer due to recrystallization, retention of water in between MgF_2 and AlF_3 crystals, surface damage, and other changes in roughness not captured by AFM, etc.

We investigated changes as a function of peel-off, time, and logarithmic time. For our comparison, we used Control 1 to compare with the formulation-applied samples. The control had a baseline growth of +0.0106 nm/peel-off. Sample S1 was observed to have the fastest growth (+71% vs control). S2 exhibited the slowest growth (-60% vs control). Meanwhile, S4 was observed to have decreases in the MgF_2 with each application. The best formulations based on our results in terms of peel-off are S2 in terms of the MgF_2 layer and S3 in terms of the Al_2O_3 layer. Note further that our

analysis of thickness evolution over time suggests that the growth is likely not linear. Log-time models fit the growth better with a higher Akaike's Information Criteria (887.94 for time dependence vs 958.93 for log-time dependence). S1 showed the fastest growth for both models, while S4 showed the most consistent decrease.

Overall, S2 was the formulation that maintained the least change in apparent MgF_2 thickness. S3 was the formulation that had the most similar MgF_2 thickness increase as the control. Both showed negligible oxide growths. The apparent MgF_2 growth rates are significant; they represent not only the MgF_2 layer, but also the presence of physically adsorbed molecules, such as adventitious carbon. If FUV reflectance remains high, then either S2 or S3 would be suitable for storage of MgF_2 on Al mirrors as well as starting paces for polymer optimization processes.

5. SUMMARY AND CONCLUSIONS

Our SE study identified two (S2 and S3) of the four FCP formulations capable of successfully cleaning thin Al+$XeMgF_2$ coatings multiple times. All formulations can be used to clean Al+$XeMgF_2$ coatings at least once. S2 and S3 also show promise as acting as protective coatings for such mirrors for at least five months storage in dry environments. Statistical analysis also confirmed that S2 and S3 were the best formulations for cleaning and storage. The Al layer thickness in the coatings studied are only 30% of flight mirror thickness and 70% of the target fluoride layer. Thus, studies on fully thick mirrors need to be completed. If, in future studies, FUV reflectance is shown to remain high, then either S2 or S3 would be suitable for storage of MgF_2 on Al mirrors under dry conditions.

S1 showed some changes in the MgF_2 layer that could indicate roughening or surface damage. This would be potentially detrimental to the surface. Degradation with S4 may also indicate that polymer-to-surface adhesion could be too high for the Al+$XeMgF_2$ film surfaces. Alternatively, giving attention to ensuring good cleaning to promote adequate adhesion prior to deposition may solve this situation. It was also observed that the changes that occur to the fluoride layer likely have a logarithmic relationship with time for samples stored in FCP.

An optimal polymer for Al+$XeMgF_2$ mirrors would also need to ensure that polymer-to-surface adhesion is in the range to remove contaminants without causing Al+$XeMgF_2$ surface damage. In addition to their present application, S2 and S3 would be useful starting formulations for Al+$XeMgF_2$ as a new formulation is designed for storing MgF_2 or other fluoride surfaces in 40% relative humidity which is characteristic of cleanrooms and environments where electronics are used.

ACKNOWLEDGMENTS

NASA SBIR (Contract #80NSSC24PB405) partially funded this research. We thank Dr. Manuel Quijada, Javier del Hoyo, Edward Wollack, and Mateo Batkis at NASA Goddard as well as Dr. Luis Rodiguez de Marcos at the Catholic University of America for providing the Al+$XeMgF_2$ samples used in this study. The authors gratefully acknowledge the J.A. Woollam Co., Inc. providing several one-year licenses for their CompleteEase software. This allowed us to analyze the many Ψ and Δ files this study generated. This work, including RA funding for students, was provided by the Department of Physics and Astronomy and the College of Computation, Mathematics and Physical Sciences of Brigham Young University.

AUTHOR DECLARATIONS

Disclosures:
Dr. James Hamilton is the CEO of Photonic Cleaning Technologies, which produces and sells First Contact Polymer.

DATA AVAILABILITY

Data have been archived locally and are available upon reasonable request.

REFERENCES

[1] Tumlinson J., Aloisi A., Kriss G., France K., Mccandliss S., Sembach K., Fox A., Tripp T., Jenkins E., Beasley M., Danforth C., Shull M., Stocke J., Lehner N., Howk C., Froning C., Green J., Oliveira C., Fullerton A., Blair B., Kruk J., Sonneborn G., Penton S., Wakker B., Prochaska X., Vallerga J., and Scowen P., "Light and Metals from Population III Stars," *ESO Astrophysics Symposia*, vol. 9, pp. 185–186, Springer-Verlag, (2012); doi:10.48550/ARXIV.1209.3272

[2] Hansen P., Townsend J., and Hedgeland R., "Lessons learned from the Hubble Space Telescope (HST) contamination control program," Journal of the IEST, vol. 50, no. 1, pp. 44–60, (2007); doi:10.17764/jiet.50.1.c7835r3280617256

[3] Stewart E., "The James Webb Space Telescope: contamination control and materials," Systems Contamination: Prediction, Control, and Performance 2018, vol. 9, pp. 16, SPIE, (2018); doi:10.1117/12.2319687

[4] Quijada M., Del Hoyo J., Rodriguez-De-Marcos L., Wollack E., Batkis M., Lewis D., Rydalch T., and Allred D., "Enhanced far ultra-violet optical properties of physical vapor deposited aluminum mirrors through fluorination," Space Telescopes and Instrumentation 2024: Ultraviolet to Gamma Ray, vol. 8, pp. 152, SPIE, (2024); doi:10.1117/12.3021592

[5] Quijada M. A., de Marcos L. V. R., Del Hoyo J. G., Gray E., Wollack E. J., and Brown A., "Advanced Al mirrors protected with LiF overcoat to realize stable mirror coatings for astronomical telescopes," SPIE Proceedings, vol. 12188, pp. 674–682, (2022); doi:10.1117/12.2630585

[6] Tuttle S., Matsumura M., Ardila D., Chen P., Davis M., Ertley C., Farr E., Fleming B., France K., Froning C., Grisé F., Hamden E., Hennessy J., Hoadley K., Mccandliss S., Miles D., Nikzad S., Quijada M., Ravi I., De Marcos L., Scowen P., Siegmund O., Vargas C., Vorobiev D., and Witt E., "Ultraviolet Technology to Prepare for the Habitable Worlds Observatory," (2024); doi:10.48550/ARXIV.2408.07242

[7] Stahl H., "Assessment of near-angle scatter on exo-Earth coronagraphy," UV/Optical/IR Space Telescopes and Instruments: Innovative Technologies and Concepts XI, vol. 10, pp. 25, SPIE, (2023); doi:10.1117/12.2676543

[8] Phelps M., Gushwa K., and Torrie C., "Optical contamination control in the Advanced LIGO ultra-high vacuum system," SPIE Proceedings, vol. 11, (2013); doi:10.1117/12.2047327

[9] Vawdrey J., Hamilton J., and Allred D., "Variable-angle, spectroscopic ellipsometry study on the repeated application of first contact polymer on silicon-based surfaces," Current Developments in Lens Design and Optical Engineering XXIV, vol. 10, pp. 24, SPIE, (2023); doi:10.1117/12.2692390

[10] Rydalch T., Lewis D., and Allred D., "Stability of lithium fluoride thin films as a function of humidity and temperature," Advances in Optical and Mechanical Technologies for Telescopes and Instrumentation V, vol. 8, pp. 207, SPIE, (2022); doi:10.1117/12.2630514

[11] Vawdrey J., Hamilton J., Watson D., Miner L., Amienghemhen O. D., Paxtonand W., and Allred D., "Effect of the repeated application of First Contact™ polymer on xenon-difluoride passivated lithium fluoride on aluminum surfaces for space telescopes," J. Vac. Sci. Technol. A., vol. 43, (2025); doi: 10.1116/6.0004601

[12] "CRC Handbook of Chemistry and Physics," pp. 313–576, CRC Press., (2016); doi:10.1201/9781315380476-3

[13] Rydalch T., "Stability and oxidation of Al mirrors coated with Xe-passivated LiF thin films," (2024). Master's thesis, Brigham Young University.

[14] Hilfiker J., Singh N., Tiwald T., Convey D., Smith S., Baker J., and Tompkins H., “Survey of methods to characterize thin absorbing films with spectroscopic ellipsometry,” Thin Solid Films, vol. 516, no. 22, pp. 7979–7989, (2008); doi:10.1016/j.tsf.2008.04.060

[15] Woollam J. and Snyder P., “Fundamentals and applications of variable angle spectroscopic ellipsometry,” Materials Science and Engineering: B, vol. 5, no. 2, pp. 279–283, (1990); doi:10.1016/0921-5107(90)90069-n

[16] Woollam J., Johs B., Herzinger C., Hilfiker J., Synowicki R., and Bungay C., “Overview of variable-angle spectroscopic ellipsometry (VASE): I. Basic theory and typical applications,” SPIE Proceedings, vol. 7, (1999); doi:10.1117/12.351660

[17] Johnson B., Avval T., Turley R., Linford M., and Allred D., “Oxidation of aluminum thin films protected by ultrathin MgF_2 layers measured using spectroscopic ellipsometry and X-ray photoelectron spectroscopy,” OSA Continuum, vol. 4, no. 3, pp. 879–895, Feb. (2021); doi: 10.1364/OSAC.417302

[18] Tompkins H. G., Tasic S., Baker J., and Convey D., “Spectroscopic ellipsometry measurements of thin metal films,” Surface and Interface Analysis, (2000); doi: 10.1002/(SICI)1096-9918(200003)29:3<179::AID-SIA701>3.0.CO;2-O

[19] Nguyen H., An I., and Collins R., “Evolution of the optical functions of thin-film aluminum: A real-time spectroscopic ellipsometry study,” Physical Review B, vol. 47, no. 7, pp. 3947–3965, (1993); doi: https://doi.org/10.1103/PhysRevB.47.3947

[20] Nečas D. and Klapetek P., “Gwyddion: an open-source software for SPM data analysis,” Open Physics, vol. 10, no. 1, pp. 181–188, (2011); doi:10.2478/s11534-011-0096-2

[21] Bruggeman D., “Berechnung verschiedener physikalischer Konstanten von heterogenen Substanzen. I. Dielektrizitätskonstanten und Leitfähigkeiten der Mischkörper aus isotropen Substanzen,” Annalen der Physik, vol. 416, no. 7, pp. 636–664, (1935); doi:10.1002/andp.19354160705

[22] Allred D. D., Turley R. S., Thomas S. M., Willett S. G., Greenberg M. J., and Perry S. B., “Adding EUV reflectance to aluminum-coated mirrors for space-based observation,” UV/Optical/IR Space Telescopes and Instruments: Innovative Technologies and Concepts VIII, vol. 10398(34), SPIE, (2017); doi: https://doi.org/10.1117/12.2274694

[23] Shah D., Patel D., Roychowdhury T., Jacobsen D., Erickson J., and Linford M., “Optical function of atomic layer deposited alumina (0.5–41.0 nm) from 191 to 1688 nm by spectroscopic ellipsometry with brief literature review,” Surface Science Spectra, vol. 26, no. 2, (2019); doi:10.1116/1.5114827

[24] Querry, Marvin R., Wieliczka David M., and Segelstein, David J., “Water (H_2O),” in Palik E. and Hunter W., Handbook of Optical Constants of Solids-II, Academic Press, San Diego, Calif. pp. 1071, (1991). ISBN 978-0-12-544422-4

[25] T. W. Marin, K. Takahashi, and D. M. Bartels, “Temperature and density dependence of the light and heavy water ultraviolet absorption edge,” J. Chem. Phys. 125(10), 104314 (2006). As cited in Lars Kröckel and Markus A. Schmidt, "Extinction properties of ultrapure water down to deep ultraviolet wavelengths," Opt. Mater. Express 4, 1932-1942 (2014) https://doi.org/10.1364/OME.4.001932